

Laboratory Experiments on the Motion of Dense Dust Clouds in Protoplanetary Disks

NICLAS SCHNEIDER¹ AND GERHARD WURM¹

¹*Faculty of Physics
University of Duisburg-Essen
Lotharstr. 1, 47057 Duisburg, Germany*

(Received 2019 September 11; Revised 2019 October 30; Accepted 2019 November 8; Published 2019 November 27)

Submitted to The Astrophysical Journal Letters

ABSTRACT

In laboratory experiments, we study the motion of levitated, sedimenting clouds of sub-mm grains at low ambient pressure and at high solid-to-gas ratios ϵ . The experiments show a collective behavior of particles, i.e. grains in clouds settle faster than an isolated grain. In collective particle clouds, the sedimentation velocity linearly depends on ϵ and linearly depends on the particle closeness C . However, collective behavior only sets in at a critical value ϵ_{crit} which linearly increases with the experiment Stokes number St . For $St < 0.003$ particles always behave collectively. For large Stokes numbers, large solid-to-gas ratios are needed to trigger collective behavior, e.g. $\epsilon_{\text{crit}} = 0.04$ at $St = 0.01$. Applied to protoplanetary disks, particles in dense environments will settle faster. In balance with upward gas motions (turbulent diffusion, convection) the thickness of the midplane particle layer will be smaller than calculated based on individual grains, especially for dust. For pebbles, large solid-to-gas ratios are needed to trigger instabilities based on back-reaction.

Keywords: Planet formation — Protoplanetary disks — Laboratory astrophysics

1. INTRODUCTION

Planet formation starts with sticking collisions of dust in protoplanetary disks (Blum & Wurm 2008). Relative velocities between the solids are provided by sedimentation to the midplane, radial and transversal drifts, and turbulence (Birnstiel et al. 2016). Collisional grain growth might proceed at least to millimeter grain size before bouncing dominates the outcome of a collision (Zsom et al. 2010; Demirci et al. 2017).

It is the interaction or coupling between the solid grains and the gas that sets the collision velocities. Beyond collisions, gas-grain coupling also determines the dust scale height or how far particles sediment to the midplane in balance with turbulent mixing (Birnstiel et al. 2016; Pignatale et al. 2017). Gas-grain coupling is also important for the radial inward drift, especially of decimeter- to meter-sized bodies (Weidenschilling 1977), and it is a major part in trapping particles in pressure bumps (Whipple 1972). While for some aspects particles can be considered as tracer particles – individual

grains with no influence on the gas motion itself – dense particle clouds require a more complex treatment.

In recent years, particle-gas feedback was suggested to promote particle concentration that eventually lead to gravitational collapse into planetesimals (Youdin & Goodman 2005; Johansen & Youdin 2007; Gonzalez et al. 2017; Dipierro et al. 2018; Squire & Hopkins 2018). Concentration mechanisms depend strongly on the particles' Stokes numbers, the metallicity, and the solid-to-gas ratio (e.g. Bai & Stone (2010); Carrera et al. (2015); Yang et al. (2017); Squire & Hopkins (2018)). In any case, these mechanisms might take over from collisional growth at pebble size to form planetesimals.

Assisting this numerical work relying on particle-gas feedback mechanisms, we investigate the motion of dense particle clouds in a thin gas in laboratory experiments here.

A basic concept in a simple system of one particle in an unlimited reservoir of gas is that the grain needs a certain gas-grain friction time τ_f to follow any change in gas motion or react to any external force and reach equilibrium between external force and friction. The flow around the particle can be divided in molecular flow ($Kn \gg 1$) determined by Epstein drag and continuum flow ($Kn \ll 1$) determined by Stokes drag where Kn

Corresponding author: Niclas Schneider
niclas.schneider@uni-due.de

is the Knudsen number with the mean free path λ and particle radius r ,

$$\text{Kn} = \frac{\lambda}{r}. \quad (1)$$

The stationary sedimentation speed of a grain is given by

$$v_0 = \tau_f \cdot g, \quad (2)$$

where g is the gravitational acceleration, i.e. the vertical component of a star's gravity in a protoplanetary disk.

The motion of an individual particle in a cloud of many particles can only be treated this way to a certain limit. It requires that back-reaction on the gas and feedback from this back-reaction to the other grains can be neglected. This is only true for an isolated particle, i.e. for low solid-to-gas mass ratios and low volume filling factors. In protoplanetary disks, the canonical solid-to-gas ratio of 0.01 can change by sedimentation and other concentration mechanisms by several orders of magnitude, while the volume filling factor remains low ($< 10^{-6}$) (Klahr et al. 2018).

Grains in a dense cloud might just effectively behave like a larger particle, moving faster like the individual grains (Johansen & Youdin 2007). Eventually, collective behavior might lead to planetesimal formation (Johansen et al. 2007; Chiang & Youdin 2010; Klahr et al. 2018).

In Schneider et al. (2019), we studied the transition from test particle to collective behavior in a levitation experiment, analyzing the free-fall velocity of grains in a cloud. We empirically found that the sedimentation velocity depends on what we call sensitivity factor F_S and the closeness C of the individual particle as

$$v_s = v_0 + F_S \cdot C. \quad (3)$$

The closeness C of a particle is constructed from the interparticle distances $r_j - r$ between the grain and all other particles j as

$$C = \sum_{j=1}^N \frac{1}{|r_j - r|} \quad (4)$$

N is the total number of particles. The sensitivity factor F_S in eq. 5 depends on the average solid-to-gas ratio ϵ of the system:

$$F_s = \alpha(\epsilon - \epsilon_{\text{crit}}) \quad \text{for} \quad \epsilon > \epsilon_{\text{crit}} \quad (5)$$

The solid-to-gas ratio ϵ is defined as the ratio between the total dust mass and the average gas mass,

$$\epsilon = \frac{N \cdot m_p}{V \cdot \rho_g} = \frac{1}{6} \pi s^3 \frac{N \rho_p}{V \rho_g}, \quad (6)$$

where m_p is the mass of a single particle, V is the total volume covered by particles, ρ_g is the gas density in the chamber, and ρ_p is the bulk density of the individual grains, and s is the particle diameter.

As seen in eq. 5, Schneider et al. (2019) also empirically found that particles are only influenced by the other particles in a cloud if the average solid-to-gas ratio ϵ is above a threshold value ϵ_{crit} ; otherwise, $F_s = 0$ and particles sediment with v_0 .

The sensitivity α connecting the solid-to-gas ratio to the sensitivity factor in eq. 5 was just a constant in Schneider et al. (2019).

This description is purely empirical and was deduced from a single experiment so far. Here, we present a systematic analysis, where we varied the gas pressure, particle size, and rotation frequency of the chamber and improved the setup and data acquisition.

2. LEVITATION EXPERIMENT

2.1. Setup

The setup of the experiment (see fig. 1) follows the principle used in aggregation experiments by Poppe & Blum (1997) and Blum et al. (1998), but is especially based on earlier experiments on dense clouds by Schneider et al. (2019).

Particles – in this study, hollow glass spheres of different sizes and densities – are dispersed once at the beginning of the experiment, within a rotating vacuum chamber with low ambient pressure. Particles are injected using a vibrating sieve in an extension of the vacuum chamber. The gas inside follows the rigid rotation of the chamber. The vacuum chamber has a diameter of 320 mm. Inside the chamber, a ring of LEDs is used to illuminate the particles. The scattered light of the particles is detected by two non-rotating cameras.

These cameras observe the particles from the front at a distance of 40 cm on a 1", 5 megapixel sensor with a spatial resolution in the order of 10 μm . The frame rate is 40 fps with an exposure time of 6 ms. The field of view is 19 \times 15 cm. Imaging and synchronization of both cameras are controlled by a machine vision computer. Spatial calibration was realized with a calibration matrix with $\sim 10,000$ data points for each camera.

The experimental parameters are the particle radius of the sample r_p , the particle bulk density ρ_p , the gas pressure p , and the rotation frequency f . We define the Stokes number of the experiment as

$$\text{St} = \tau_f \cdot f. \quad (7)$$

The friction time is calculated with equation 2. The experiments were carried out similar to the ones described in Schneider et al. (2019). In short, the chamber was

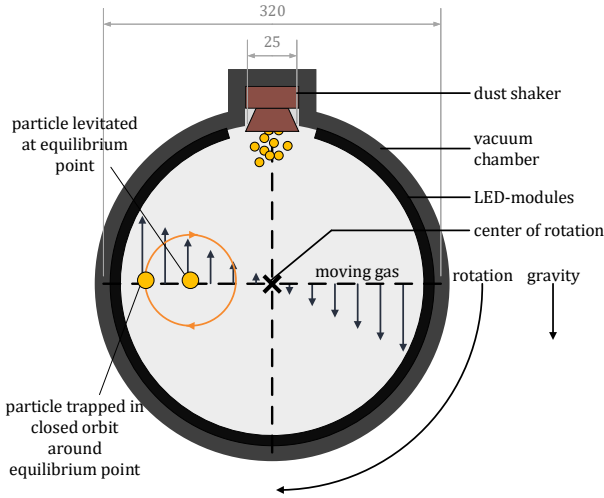


Figure 1. Experimental setup without auxiliary parts. The vacuum chamber is evacuated to a preset pressure. Two cameras observe the particles from the front. Illumination is provided by LED modules.

evacuated to a preset pressure and then disconnected from the vacuum pump. The injection process was then started and the chamber was set to a predefined rotation frequency before image acquisition for both cameras was started.

2.2. Data analysis

In principle, data were processed as in [Schneider et al. \(2019\)](#). We refer the reader to that paper for details. All particle positions were extracted for all times with Trackmate ([Tinevez et al. 2017](#)), using a Laplacian of Gaussian (LoG) particle detector and a Linear Motion LAP tracker for particle track assignment. For data analysis, all particle positions and every particle track with track length > 100 frames were taken into account.

Since we used two parallel cameras, the 3d position was reconstructed as a new feature here. The stereoscopic reconstruction was carried out by an algorithm that maps the expected particle position of the first on the second camera image and then finds matches by minimizing the difference between the projected position and detected particle positions of the second camera image.

The error in the z -position of each particle is $\sim 2\%$. From these data, individual sedimentation velocities, individual closenesses, and average solid-to-gas ratios were determined.

Furthermore, in this study, the sedimentation velocity was normalized to the undisturbed, individual sedimen-

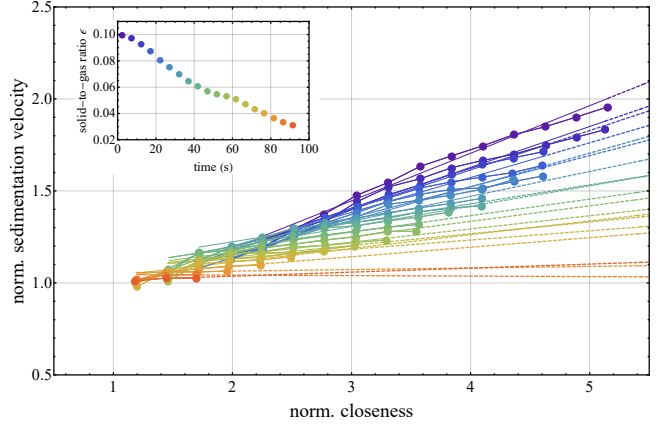


Figure 2. Normalized sedimentation velocity over normalized closeness for 19 revolutions of experiment 8 (table 1). The color of the data points refers to the revolution of the experiment chamber during the measurement starting with revolution 1 in blue (top) and revolution 19 in red (bottom). Data points are average values for at least 1000 particle positions with an equidistant spacing of the binned values in closeness space. The total number of examined single sedimentation velocity data points is about 1,025,000; the total number of examined particle positions is about 1,600,000. The top left inset shows the solid-to-gas ratio of each revolution as a function of time.

tation velocity of the grains used in the experiment v_0 . The closeness was normalized by multiplication with the particle diameter s of the glass beads used in the corresponding experiment (table 1).

According to equation 3 and 5, the sedimentation velocity depends on the closeness C and the solid-to-gas ratio ϵ . Due to particle loss ϵ decreases with time. We group the measured particle positions and velocities in full revolutions of the experiment chamber. Fig. 2 shows an example of the sedimentation velocity over closeness. This confirms the linear dependence found in [Schneider et al. \(2019\)](#).

The slope varies with every revolution or average ϵ . According to equation 3 and 5, this slope is equal to $F_s = \alpha(\epsilon - \epsilon_{\text{crit}})$.

Fig. 3 confirms the linear trend of the sensitivity factor on ϵ ([Schneider et al. 2019](#)). From the linear fit $F_S = a \cdot \epsilon + b$, we can then deduce the sensitivity $\alpha = a$ and the critical solid-to-gas ratio ϵ_{crit} as

$$\epsilon_{\text{crit}} = -\frac{b}{a}. \quad (8)$$

We define a system to be collective when individual sedimentation velocities deviate from v_0 or if $F_S > 0$. We define a system as non-collective if all particles behave like test particles, sedimenting independently of local closeness variations.

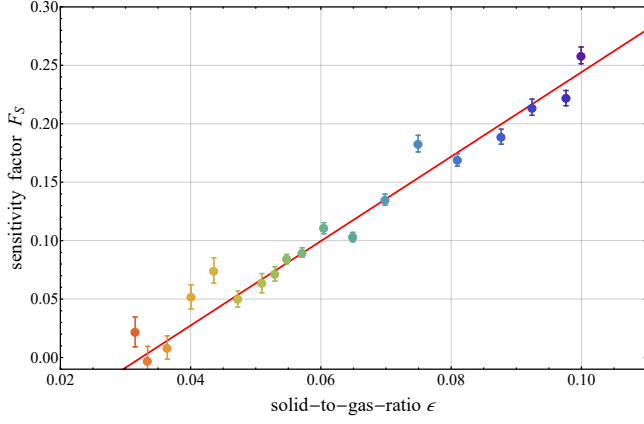


Figure 3. Sensitivity factor F_S over solid-to-gas ratio ϵ of experiment 8 (table 1). The color of the data points refers to the data points shown in fig. 2. The linear fit is $F_S(\epsilon) = -0.12 + 3.6 \cdot \epsilon$

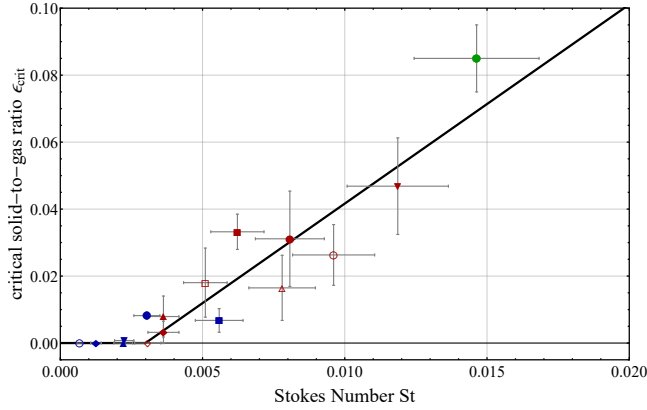


Figure 4. Critical solid-to-gas ratio of all performed experiments in dependence on the Stokes number. The shape and color of data points correspond to the experiments shown in tab. 1. Fit: $\epsilon_{\text{crit}}(\text{St}) = -0.018 + 5.9 \cdot \text{St}$

3. DISCUSSION

After data analysis, two main quantities are given: ϵ_{crit} and α . The critical solid-to-gas ratio varied for the different experiments carried out. As we also changed several parameters between individual experiments it is *a priori* not clear whether these two parameters follow systematic trends. Therefore, we considered ϵ_{crit} to depend on a number of individual variables, including Knudsen number, pressure, and particle size. However, the only systematic dependence found was concerning the experiment's Stokes number St , mainly influenced by τ_f . This is shown in fig. 4.

There is a clear linear trend in the data. Interestingly, below a Stokes number of $\text{St} \leq 0.003$, the deduced ϵ_{crit} formally becomes negative. Negative ϵ_{crit} refers to systems that are *always* collective. Since F_S always has to be larger or equal to 0, negative ϵ_{crit} are set to 0. Par-

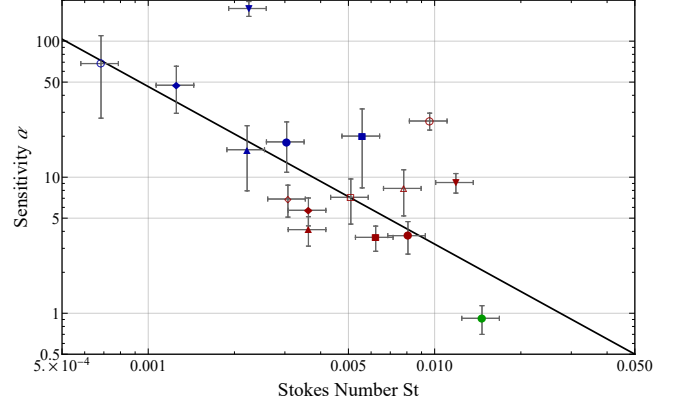


Figure 5. Sensitivity of all performed experiments in dependence on the Stokes number. The shape and color of data points correspond to the experiments shown in tab. 1. Fit: $\alpha(\text{St}) = 0.016 \cdot \text{St}^{1.2}$

ticles with $\text{St} \leq 0.003$ always back-react to the gas flow in such a manner that other particles are influenced by this.

The sensitivity α also depends on the Stokes number as shown in fig. 5. We fitted a power law to the data as one possible functional dependence. Small St particles have a higher impact on the gas flow than large St particles for the same average solid-to-gas mass ratio.

The linear dependence of the sedimentation velocity on the closeness and on the solid-to-gas ratio is found for all parameter combinations. Therefore, we consider this a robust, general finding.

4. APPLICATION TO PROTOPLANETARY DISKS

The Stokes number in protoplanetary disks is defined as $\text{St} = \tau \cdot \Omega_K$, where Ω_K is the Kepler frequency. The Stokes number below which grains always behave collectively of 0.003 corresponds to particle sizes of about 1 cm at 1 AU for a particle density of 1 g cm^{-3} in a typical disk (Johansen et al. 2014).

For larger grains, the system becomes increasingly insensitive to high solid-to-gas ratios and only turns collective for higher values of ϵ . It seems more than plausible that drag instabilities can only occur if the cloud becomes collective. Therefore, this study suggests that grains larger than 1 cm require larger ϵ to trigger drag instabilities at 1 AU or grains larger than 1 mm at 10 AU. For smaller grains, the clouds are always collective and very sensitive to changes in ϵ . Drag instabilities might therefore regularly occur for small grains rather than large grains. As grain growth proceeds in disks, pristine bodies might preferentially consist of entities of the threshold size, especially not of larger grains. This is in agreement with observations of comets (Blum et al. 2017).

5. CONCLUSIONS

Protoplanetary disks are regions with a wide range of solid–gas interactions, ranging from single test particle behavior of a dust grain in regions depleted of dust to solid dominated motion in gravitationally unstable particle subclouds. The solid-to-gas mass ratio ϵ can vary from lower than interstellar $\epsilon \leq 0.01$ to larger than $\epsilon \geq 100$, while the volumetric filling factor Φ remains below 10^{-6} . In our experiment, we confirm that the transition from test particle to collective behavior in comparably low- Φ environments is characterized by a threshold for the average solid-to-gas ratio. Above the threshold, particle feedback on the gas is high enough to influence other particles.

This threshold depends on the Stokes number of the particles. The larger the Stokes number, the higher the solid-to-gas ratio that still allows test particle behavior. On the lower Stokes number end, our experiments *always* come with collective behavior. Applied specifically to particle motion in protoplanetary disks, we would like to highlight two aspects of this work.

First, in a simple cloud of small particles, their motion can be collective already at low solid-to-gas ratios if the Stokes number is small, e.g. if grains are still dust and not yet pebbles. This, e.g., leads to increased sedimentation velocities. As the maximum dust height is

a balance between upward gas motion, e.g. as turbulent diffusion or convection, and sedimentation, faster settling corresponds to a reduced dust height for the same upward gas flow in parts behaving collectively. If this also changes the scale height observed astronomically depends on the local conditions at the respective height, i.e. if the top of the particle layer would be collective or non-collective. Collective sedimentation might also lead to a detachment of the surface layer and the midplane particles, but that is only a guess and further details are beyond the scope of this Letter.

Also, other motions will change accordingly, e.g. the radial inward drift velocity for a given grain size in a collective ensemble will change.

Second, for large grains or rather at higher Stokes numbers, ever higher solid-to-gas ratios are needed to get the cloud collective. A threshold grain size of millimeter to centimeter marks the transition between always collective and solid-to-gas ratio dependence. Drag instabilities leading to planetesimal formation will favor this particle size supporting observations of comets.

ACKNOWLEDGMENTS

This project is supported by DFG grant WU 321/16-1. We thank the two referees for a very constructive review of the paper.

APPENDIX

A. EXPERIMENTAL PARAMETERS

Experiment	Particle Size (μm)	Particle Density (kg m^{-3})	Pressure (mbar)	Rotation Frequency ($10^{-3} \times \text{Hz}$)	v_0 (mms^{-1})	Initial ϵ (10^{-3})	Kn	St (10^{-3})	Re (10^{-3})	Symbol
Schn19+	165 ± 15	60 ± 6	9.5 ± 1	336 ± 2	68 ± 7	150 ± 20	0.08 ± 0.02	14 ± 2	7 ± 2	●
1	36 ± 9	280 ± 76	8 ± 1	216 ± 2	22 ± 2	42 ± 4	0.46 ± 0.16	3.0 ± 0.5	0.4 ± 0.2	●
2	36 ± 9	280 ± 76	8 ± 1	273 ± 2	32 ± 3	41 ± 4	0.46 ± 0.16	5.6 ± 0.8	0.6 ± 0.25	■
3	36 ± 9	280 ± 76	13.5 ± 1	145 ± 2	14 ± 1	23 ± 2	0.30 ± 0.10	12 ± 0.2	0.4 ± 0.2	◆
4	36 ± 9	280 ± 76	14 ± 1	231 ± 2	15 ± 2	21 ± 2	0.26 ± 0.09	2.2 ± 0.3	0.5 ± 0.2	▲
5	36 ± 9	280 ± 76	14 ± 1	173 ± 2	20 ± 2	10 ± 1	0.26 ± 0.09	2.2 ± 0.3	0.7 ± 0.3	▼
6	36 ± 9	280 ± 76	10 ± 1	117 ± 2	9 ± 1	6.2 ± 0.6	0.37 ± 0.13	0.7 ± 0.1	0.2 ± 0.1	○
7	132.5 ± 8	75 ± 4	3.9 ± 0.4	293 ± 2	43 ± 4	145 ± 15	0.26 ± 0.04	8.0 ± 0.1	1.4 ± 0.4	●
8	132.5 ± 8	75 ± 4	3.9 ± 0.4	203 ± 2	48 ± 5	107 ± 11	0.26 ± 0.04	6.2 ± 0.9	1.6 ± 0.4	■
9	132.5 ± 8	75 ± 4	4 ± 0.4	153 ± 2	37 ± 4	56 ± 6	0.25 ± 0.04	3.6 ± 0.5	1.3 ± 0.3	◆
10	132.5 ± 8	75 ± 4	4 ± 0.4	153 ± 2	37 ± 4	98 ± 10	0.25 ± 0.04	3.6 ± 0.5	1.3 ± 0.3	▲
11	132.5 ± 8	75 ± 4	8.1 ± 1	378 ± 2	49 ± 5	68 ± 7	0.12 ± 0.02	28 ± 2	3.5 ± 0.9	▼
12	132.5 ± 8	75 ± 4	8.1 ± 1	375 ± 2	40 ± 5	51 ± 5	0.12 ± 0.02	9.6 ± 1	2.8 ± 0.7	○
13	132.5 ± 8	75 ± 4	12 ± 1	199 ± 2	40 ± 4	48 ± 5	0.08 ± 0.01	5.1 ± 0.7	4 ± 1	□
14	132.5 ± 8	75 ± 4	8.1 ± 1	160 ± 2	30 ± 3	36 ± 4	0.12 ± 0.02	3.1 ± 0.5	2.1 ± 0.5	◇
15	132.5 ± 8	75 ± 4	8.1 ± 1	297 ± 2	41 ± 4	74 ± 7	0.12 ± 0.02	8 ± 1	2.9 ± 0.8	△

Table 1. Parameters of the Laboratory Experiments. Schn19+ gives the data published in [Schneider et al. \(2019\)](#)

REFERENCES

- Bai, X.-N., & Stone, J. M. 2010, *The Astrophysical Journal*, 722, 1437, doi: [10.1088/0004-637X/722/2/1437](https://doi.org/10.1088/0004-637X/722/2/1437)
- Birnstiel, T., Fang, M., & Johansen, A. 2016, *SSRv*, 205, 41, doi: [10.1007/s11214-016-0256-1](https://doi.org/10.1007/s11214-016-0256-1)
- Blum, J., & Wurm, G. 2008, *araa*, 46, 21, doi: [10.1146/annurev.astro.46.060407.145152](https://doi.org/10.1146/annurev.astro.46.060407.145152)
- Blum, J., Wurm, G., Poppe, T., & Heim, L.-O. 1998, *Earth, Moon, and Planets*, 80, 285, doi: [10.1023/A:1006386417473](https://doi.org/10.1023/A:1006386417473)
- Blum, J., Gundlach, B., Krause, M., et al. 2017, *MNRAS*, 469, S755, doi: [10.1093/mnras/stx2741](https://doi.org/10.1093/mnras/stx2741)
- Carrera, D., Johansen, A., & Davies, M. B. 2015, *Astronomy & Astrophysics*, 579, A43, doi: [10.1051/0004-6361/201425120](https://doi.org/10.1051/0004-6361/201425120)
- Chiang, E., & Youdin, A. N. 2010, *Annual Review of Earth and Planetary Sciences*, 38, 493, doi: [10.1146/annurev-earth-040809-152513](https://doi.org/10.1146/annurev-earth-040809-152513)
- Demirci, T., Teiser, J., Steinpilz, T., et al. 2017, *ApJ*, 846, 48, doi: [10.3847/1538-4357/aa816c](https://doi.org/10.3847/1538-4357/aa816c)
- Dipierro, G., Laibe, G., Alexander, R., & Hutchison, M. 2018, *MNRAS*, 479, 4187, doi: [10.1093/mnras/sty1701](https://doi.org/10.1093/mnras/sty1701)
- Gonzalez, J.-F., Laibe, G., & Maddison, S. T. 2017, *Monthly Notices of the Royal Astronomical Society*, 467, 1984, doi: [10.1093/mnras/stx016](https://doi.org/10.1093/mnras/stx016)
- Johansen, A., Blum, J., Tanaka, H., et al. 2014, in *Protostars and Planets VI*, ed. H. Beuther, R. S. Klessen, C. P. Dullemond, & T. Henning, 547, doi: [10.2458/azu_uapress.9780816531240-ch024](https://doi.org/10.2458/azu_uapress.9780816531240-ch024)
- Johansen, A., Oishi, J. S., Mac Low, M.-M., et al. 2007, *Nature*, 448, 1022, doi: [10.1038/nature06086](https://doi.org/10.1038/nature06086)
- Johansen, A., & Youdin, A. 2007, *The Astrophysical Journal*, 662, 627, doi: [10.1086/516730](https://doi.org/10.1086/516730)
- Klahr, H., Pfeil, T., & Schreiber, A. 2018, *Instabilities and Flow Structures in Protoplanetary Disks: Setting the Stage for Planetesimal Formation*, 138, doi: [10.1007/978-3-319-55333-7_138](https://doi.org/10.1007/978-3-319-55333-7_138)
- Pignatale, F. C., Gonzalez, J. F., Cuello, N., Bourdon, B., & Fitoussi, C. 2017, *MNRAS*, 469, 237, doi: [10.1093/mnras/stx801](https://doi.org/10.1093/mnras/stx801)
- Poppe, T., & Blum, J. 1997, *Advances in Space Research*, 20, 1595, doi: [10.1016/S0273-1177\(97\)00817-X](https://doi.org/10.1016/S0273-1177(97)00817-X)
- Schneider, N., Wurm, G., Teiser, J., Klahr, H., & Carpenter, V. 2019, *The Astrophysical Journal*, 872, 3, doi: [10.3847/1538-4357/aafd35](https://doi.org/10.3847/1538-4357/aafd35)
- Squire, J., & Hopkins, P. F. 2018, *MNRAS*, 823, doi: [10.1093/mnras/sty854](https://doi.org/10.1093/mnras/sty854)
- Tinevez, J.-Y., Perry, N., Schindelin, J., et al. 2017, *Methods*, 115, 80, doi: [10.1016/j.ymeth.2016.09.016](https://doi.org/10.1016/j.ymeth.2016.09.016)
- Weidenschilling, S. J. 1977, *Ap&SS*, 51, 153, doi: [10.1007/BF00642464](https://doi.org/10.1007/BF00642464)
- Whipple, F. L. 1972, in *From plasma to planet*, 211
- Yang, C.-C., Johansen, A., & Carrera, D. 2017, *Astronomy & Astrophysics*, 606, A80, doi: [10.1051/0004-6361/201630106](https://doi.org/10.1051/0004-6361/201630106)
- Youdin, A. N., & Goodman, J. 2005, *The Astrophysical Journal*, 620, 459, doi: [10.1086/426895](https://doi.org/10.1086/426895)
- Zsom, A., Ormel, C. W., Güttler, C., Blum, J., & Dullemond, C. P. 2010, *Astronomy and Astrophysics*, 513, A57, doi: [10.1051/0004-6361/200912976](https://doi.org/10.1051/0004-6361/200912976)